# Helium-atom scattering investigation of facetting of the Al stepped (332) surface

B. J. Hinch,* A. Lock, H. H. Madden,† J. P. Toennies, and G. Witte
*Max-Planck-Institut für Strömungsforschung, Bunsenstrasse 10, D-3400 Göttingen, Federal Republic of Germany*
(Received 14 December 1989)

Helium-atom scattering has been used to study the facetting of an aluminum crystal that was cut at an angle of 10.0° from the (111) face to produce a (332) periodically stepped surface. After initial surface preparation of repeated sputtering and annealing cycles, the diffraction peak structures indicated strong facetting. Data collected for a wide range of initial He-atom wave vectors between 4.3 $\text{Å}^{-1}$ (9.7 meV) and 12.5 $\text{Å}^{-1}$ (81.8 meV) along the $[\bar{1}\,\bar{1}3]$ azimuth reveal well-formed (111), disordered (221), and a small proportion of (113) facets. The identification of facets is made relatively easy with He-atom scattering due to the large form factors for individual steps. From studies of the temperature dependence, three temperature ranges were identified. At the highest investigated surface temperatures ($T_{\text{Al}} > 650$ K), (111) and (221) facets build up and predominate. For intermediate temperatures (650 K $> T_{\text{Al}} >$ 500 K) the macroscopic (332) face begins to form. At lower temperatures the surface is sufficiently immobile to inhibit a redistribution between facets. However, (221) facets do show a temperature-dependent roughness down to 300 K. The instantaneous long-range step distribution freezes in at $T_{\text{Al}} \leq 500$ K.

## I. INTRODUCTION

Vicinal surfaces have been frequently studied because of their relatively high density of step edges. The density of steps is simply determined by the orientation, i.e., the Miller index, of the surface. High-index faces appear to be a good connecting link between ideal flat surfaces and real surfaces which have defects such as steps and kinks.

Steps are generally believed to be active sites for catalysis.[1] Step edges are also assumed to have associated strain fields that locally affect surface reconstructions or adsorbate superlattices.[2,3] Furthermore, steps may act as nucleation centers for growth or ordering processes.[4] Stepped surfaces invariably have different characteristics than their nonstepped counterparts in phase transitions,[5] and only rarely has it been found that steps have no influence on the lateral coherence of superstructures.[6]

In the past few years vicinal surfaces have also been frequently studied because they show a roughening transition. This phase transition is continuous with increasing temperature and is accompanied by an increased disorder of the edges and variations in the step density. As a result of the high density of steps on these surfaces the characteristic temperatures of this transition are sufficiently reduced to be easily accessible. The high surface sensitivity of He-atom scattering (HAS) has been used to study the roughening of fcc $(11m)$ faces $(m=3,5,7,11)$.[7,8] From these measurements, step-step–interaction and kink-formation energies have been estimated. On many stepped surfaces another form of topographical surface change occurs. Some surface orientations tend to be thermodynamically unstable and will decompose into stable facets.[9]

Facetting is observed on clean surfaces as well as on adsorption or segregation of contaminants, and has been reported for Pt,[10–13] Pd,[14] Ni,[15,16] Cu,[17–19] and Au (Refs. 20 and 21) surfaces.

Here we present the results of an investigation of the Al (332) vicinal surface using HAS. The surface was observed to facet to (111), (113), and (221) faces, the latter pair of which [just as the (332) surface] can still be described as vicinal to the (111) face. The HAS technique is particularly suited to the identification of this combination of facets. The thermal stability of this surface and the related facets have been investigated, and three distinct temperature regimes have been identified. Possible driving forces for the facetting process are discussed.

## II. SURFACE PREPARATION AND LOW-ENERGY ELECTRON DIFFRACTION RESULTS

An aluminum crystal was cut to within 0.2° of the (332) face, the geometry of which is illustrated in Fig. 1. The surface was mechanically polished and was then transferred to an ultrahigh vacuum (UHV) chamber, which had a base pressure lower than $1\times10^{-10}$ mbar. The initial cleaning procedure involved repeated cycles of 1-keV $Ar^+$ bombardment (30–40 min) and heating to 780 K (3–5 min). After about 25 cycles the cylindrical-mirror-analyzer Auger signals showed contamination levels of carbon ([C] < 0.3 at. %), sulfur ([S] < 0.1 at. %), and oxygen ([O] ~ 0.4 at. %).

The crystal was then removed to another UHV apparatus, which was used for the He-atom-diffraction experiments. This apparatus will shortly be described in detail,[22] but we give a brief description here. The design aspects associated with atom diffraction are essentially very similar to another apparatus described elsewhere.[23] The supersonic helium-atom source may be maintained at temperatures $T_0$ between 45 and 350 K. The resulting beams have velocity spreads $(\Delta v/v)$ of about 1% with wave vectors between $k_i = 4.3$ $\text{Å}^{-1}$ (9.66 meV) and $k_i = 12.51$ $\text{Å}^{-1}$ ( 81.8 meV). The atoms are scattered

 

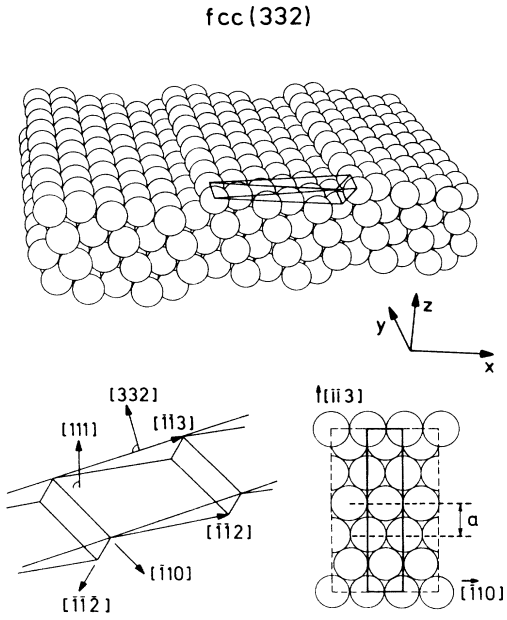


FIG. 1. Ball model and graphical representations of the fcc (332) surface. Each rectangular unit cell consists of a (111) terrace and a step edge oriented along the $[\bar{1}10]$ direction. The $x$, $y$, and $z$ axes are defined with respect to the (111) terrace direction. The row spacing, $a$, in this coordinate frame along the $x$ direction is illustrated in the lower right-hand inset. The tilted coordinate frame, denoted in the text by subscripts $\parallel$ and $\perp$, are depicted with respect to the macroscopic surface directions, $[\bar{1}\,\bar{1}\,3]$ and [332], respectively.

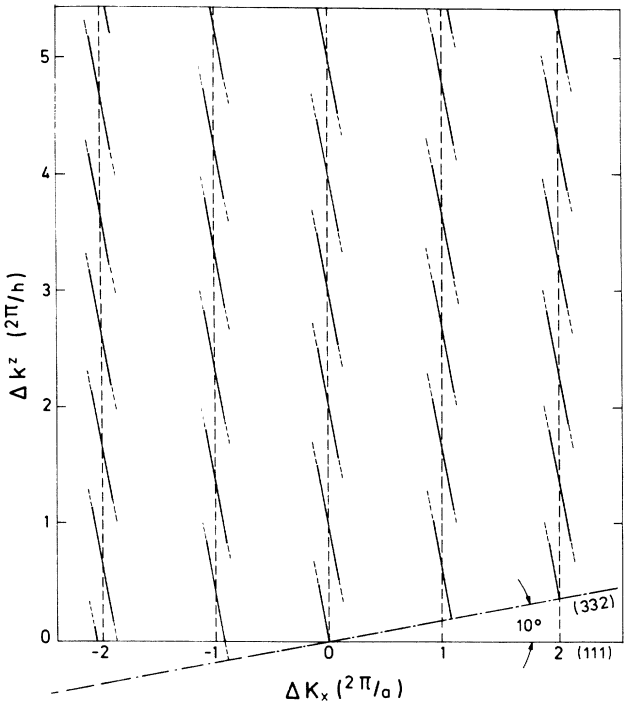


FIG. 2. Solid lines show the positions of intensities observable with LEED in the simplest of kinematic approximations for an ideal (332) vicinal surface. The vertical dashed lines indicate the two-dimensional (2D) Bragg conditions of a (111) surface, $\Delta K_x = G_x = n2\pi/a$ ($a$ is defined in Fig. 1). The tilted dashed-dotted line at the base represents the angle of inclination of the macroscopic surface. The perpendicular momentum transfers, $\Delta k^z$, are denoted in units of $2\pi/h$, where $h$ is the height (in the $z$ direction) of each step on the (111) terraces.

through a fixed angle of 91.5° and detected by a magnetic mass spectrometer using electron-bombardment ionization and pulse counting. Angular scans are made by rotating the crystal target about an axis perpendicular to the plane of the incident and final scattered beams. The overall angular resolution of the apparatus, which depends on the incident beam and detector geometry, was calculated using the method of Hinch, Frankl, and Allison[24] to be approximately 0.33°. This is in good agreement with the full width at half maximum of the sharpest experimental peak, which was 0.35°. The incident angle can be measured with a resolution of 0.04°. Most of the angular scans were taken at angles in steps of 0.1°, and after many angular scans over the whole angular range the diffraction-peak positions were found to be reproducible to 0.1°. The target chamber has a base pressure of less than $8\times10^{-11}$ mbar. The apparatus is equipped with low-energy electron diffraction (LEED) and a Leybold-Hereaus EA11 electron-energy analyzer and x-ray and ultraviolet light sources. The same cleaning procedure discussed above was resumed to remove contamination arising from the short exposure to atmosphere. The final cleaning cycles were typically of 1 h sputtering at room temperature with a 1-keV $Ar^+$ beam (2 $\mu A\,cm^{-2}$), followed by crystal temperature flashes to 750 K. Studies of the Mg $K\alpha$–radiation–induced electron spectra revealed contaminant levels for O of the order of 1%, while no contamination signals for C or S ($<0.2$ and $<0.1$ at. %, respectively) were seen.

Figure 2 shows schematically the reciprocal-lattice rods that one would expect with LEED for a perfect stepped crystal. It should be noted that the momentum transfers perpendicular to the surface, $\Delta k^z$, and parallel to the surface, $\Delta K_x$, of Fig. 2 are referenced to the planes of the (111) terraces and displayed in units of $2\pi/h$ and $2\pi/a$, respectively. These units are defined in the caption of Fig. 2. The alternative coordinate system, referenced to the macroscopic (332) surface, is rotated through 10.0°. In this coordinate frame the perpendicular and parallel momentum transfers will be referred to as $\Delta k_\perp$ and $\Delta K_\parallel$, respectively. This notation will be used throughout this paper. Figure 3 shows the actually observed LEED pattern. The peak splittings compared to the ideal crystal (Fig. 2) are replaced by broad diffuse peaks. Sharp peaks were found only at the three-dimensional (3D) Bragg-scattering conditions. This type of pattern is of the type expected from a rough (111) surface having a high density of irregularly spaced step edges.[25] Despite a relative 10° misorientation, the present LEED apparatus was not able to distinguish this system from a rough (111) surface.

## III. STRUCTURAL DETERMINATION FROM HAS ANGULAR DISTRIBUTIONS

Most of the data to be presented are the result of scattering along the $[\bar{1}\,\bar{1}\,3]$ azimuth, which is uphill per-

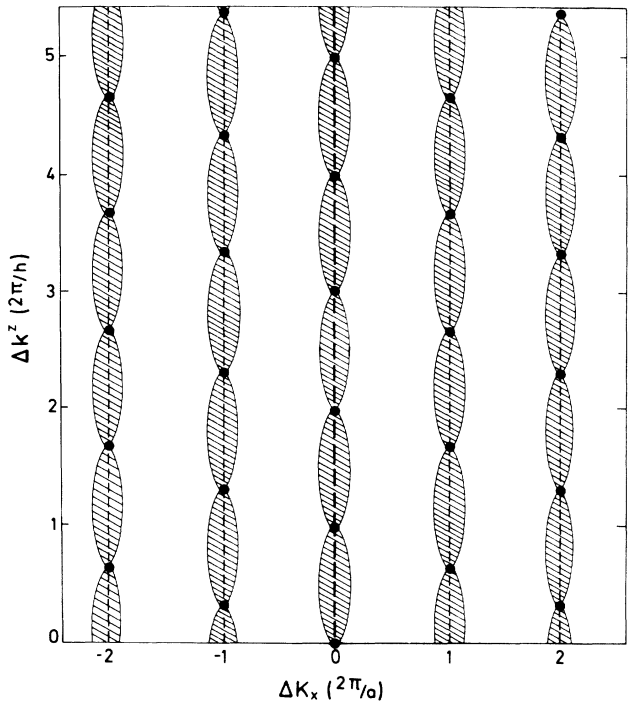


FIG. 3. Diffraction pattern expected with kinematic LEED from a rough, randomly stepped (111) surface. The largest intensities and sharpest peaks are to be found at the 3D Bragg conditions (solid dots).

pendicular to the step edges, as illustrated in the inset of Fig. 4. A typical angular scan, as shown in Fig. 4, was made by rotating the crystal face through 90° about an axis perpendicular to the plane defined by the incident wave vector $\mathbf{k}_i$ and final wave vector $\mathbf{k}_f$. Grazing incidence corresponds to an incident scattering angle $\theta_i \approx 90°$ with respect to the normal. In this case the atoms strike deep into the step risers.

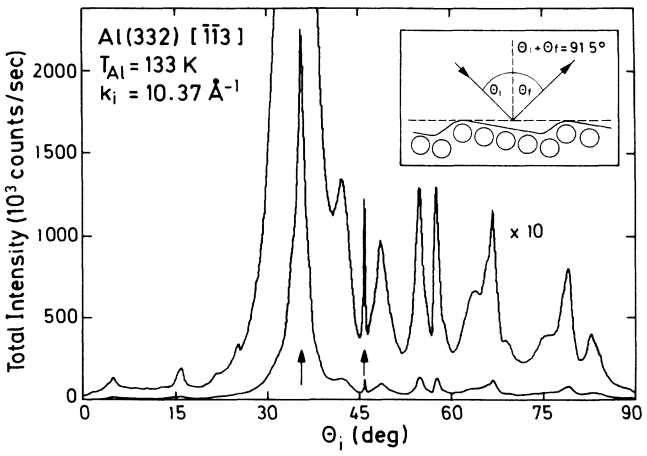


FIG. 4. Experimental HAS angular distribution showing total integral diffraction intensities along the $[\bar{1}\,\bar{1}\,3]$ azimuth. The specular scattering from the macroscopic surface is observed at $\theta_i = 45.77°$, whereas the specular peak from the terraces appears at $\theta_i = 35.75°$.

The peak of largest intensity of Fig. 4, at $\theta_i = 35.7°$, is in the specular direction of the (111) planes ($\Delta K_x = 0$). Note that on stepped surfaces the largest intensity is not in the specular direction of the macroscopic surface ($\Delta K_{\parallel} = 0$). As in the LEED patterns taken in the same apparatus, the (111) specular peak was never split, as would be expected for a regular array of step edges.

Figure 5 shows the intensity of this specular peak as a function of the elastic perpendicular momentum exchange, $\Delta k^z = (\mathbf{k}_f^z - \mathbf{k}_i^z)$, where

$$\Delta k_{\rm el}^z = k_i(\cos\theta_f + \cos\theta_i) \ . \tag{1}$$

This plot is called a "drift" spectrum, as it involves a controlled linear drift of the helium-beam-source temperature $T_0$ and a change in the incident wave vector $k_i \propto T_0^{1/2}$ with time. He-atom-scattered intensity is measured at regular intervals corresponding to points along the $\Delta K_x = 0$ reciprocal-lattice rod (e.g., see Fig. 2). The intensities have not been corrected for the slow falloff of He flux, nor for the increased Debye-Waller effect and greater attenuation, with increasing source temperature. Three maxima are observed corresponding to $\Delta k^z = 8.01$, 10.70, and 13.33 Å$^{-1}$, which are spaced at intervals of 2.69 and 2.63 Å$^{-1}$. As discussed in the following section, these maxima are attributed to constructive interference at 3D Bragg points. The smooth regular form of the minima in the oscillations and the observed spacing are consistent with a rough (111) surface having many monatomic steps.[26] The step height $h = 2.36$ Å as calculated from the relationship $h = n2\pi/\Delta k^z$ is consistent with the crystallographic spacing of (111) planes of 2.34 Å. A significant number of steps of larger heights, which would show up as additional peaks of smaller spacing was not observed. Evidence for selective-adsorption bound-state resonances as seen in analogous experiments on LiF (Ref.

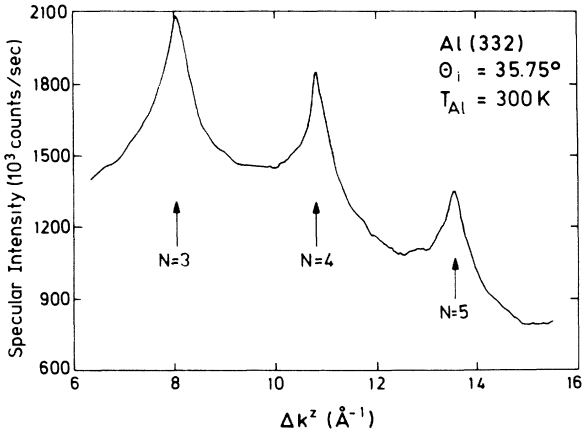


FIG. 5. Specular intensity measured at fixed scattering angles for varying incident He-beam energies in the range 9.6–67.5 meV. The total perpendicular momentum transfer $\Delta k^z$ for the elastic terrace specular peak ($\Delta K_x = 0$) was evaluated from time-of-flight measurements taken at regular intervals of the incident wave vector $k_i$. The three observed maxima correspond to the 3D Bragg conditions. For the terrace specular direction, $\Delta k^z = n2\pi/h$ [see Fig. 2(b)].

27) is also not apparent. As we shall see later, this is probably due to the highly disordered surface condition and/or to the very large number of open diffraction channels of the stepped surface.

The minima in the oscillations of the drift measurement will depend on the angular resolution (see Sec. II) since it is related to a broadening of the (111) specular peak and the resulting reduction in the peak intensities. At no stage does the intensity vanish entirely, as predicted by kinematic models of scattering from an ideal vicinal (332) surface[25] (see Fig. 2). This lack of a vanishing between 3D Bragg points is also consistent with the absence of the splitting of the specular peak.

More extensive information is provided by an analysis of many angular distributions measured for different values of the incident wave vector in a plane perpendicular to the steps. Over 30 angular distributions similar to Fig. 4 were measured for surface temperatures of $T_s < 150$ K for a wide range of incident wave vectors between 4.3 $\text{Å}^{-1}$ (9.7 meV) and 12.5 $\text{Å}^{-1}$ (81.8 meV). This large amount of data is summarized in Fig. 6, where the reciprocal-space positions of all identifiable peaks are plotted in a diagram of $\Delta k^z$ versus $\Delta K_x$. This diagram reveals the presence of peaks between $\Delta K_x = 2n\pi/a = G_x$ rods of the reciprocal lattice of the Al(111) terraces. Three unequivocal sets of parallel reicprocal-lattice rods running through all peak-intensity positions have been identified. Both the angles of inclination, with respect to the [111] direction, and their separations in reciprocal space, provide direct evidence for three types of facets on the nominal (332) surface. In this way we have identified facets with (113), (111), and (221) structures, but, in fact, no facets with the nominal (332) structure from scattering in one plane only.

The small arcs of circles drawn through many points of Fig. 6 represent one-third of the full width at half maximum (FWHM) of the associated peak. Points with no arc drawn represent peaks that were too narrow for the peak width to be apparent in Fig. 6. The limited number of points which are not on the reciprocal-lattice rods of the (221), (111), and (113) facets of Fig. 6 are largely accounted for by realizing that two or more broad peaks will not be clearly separable if their widths are too large.

Figure 7 shows the geometrical structure of the identified facets. The (221) surface has a very similar structure to that of the (332) surface, but has a higher step density, $\rho_s$, where $\rho_s$ is defined as the number of steps per unit distance in the $x$ direction. The (113) face has an even higher density of steps, but in the opposite orientation with respect to the (111) terraces. The intensities of the (113)-related diffraction peaks are relatively small, and hence the relative proportion of the (113) facets is also expected to be small. For simplicity in the present discussion this total fraction, $f_{(113)}$, and the fraction of facets other than (332), (221), and (111) will be assumed to be zero. A relationship between the proportions of (111) and (221) facets, $f_{(111)}$ and $f_{(221)}$, respec-

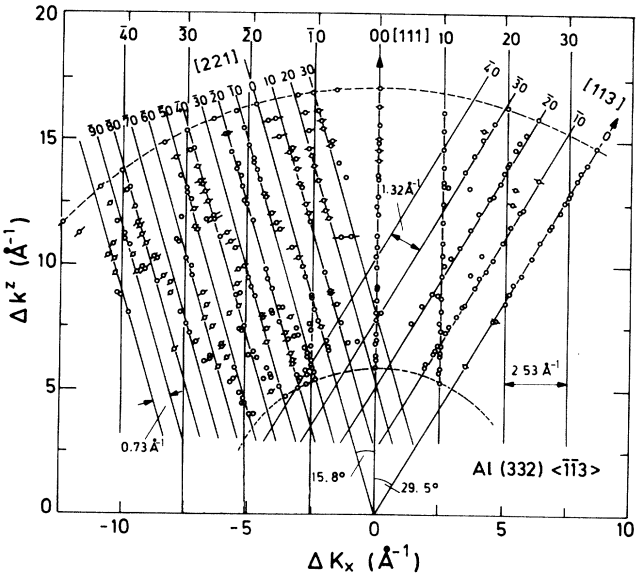


FIG. 6. Circles indicate the positions of all peak maxima observed with angular scan measurements from the crystal at temperatures of 150 K or slightly below. An individual scan describes an arc of circle in reciprocal-lattice space. For this scattering geometry, the scan with lowest incident energy (9.6 meV) describes a circle of radius 6.08 $\text{Å}^{-1}$, and that with highest incident energy (74.8 meV), a circle of radius 16.91 $\text{Å}^{-1}$. The solid lines are the reciprocal-lattice rods from (221), (111), and (113) facets of the surface. The uppermost part of the figure displays the diffraction order of each reciprocal-lattice rod. Short dashes through circles illustrate the angular range corresponding to $\frac{1}{3}$ of the FWHM of each peak. Many peaks are very sharp, showing little or no broadening. This is indicated simply by the absence of dashes. Note that the intensities of the peaks vary over orders of magnitude.

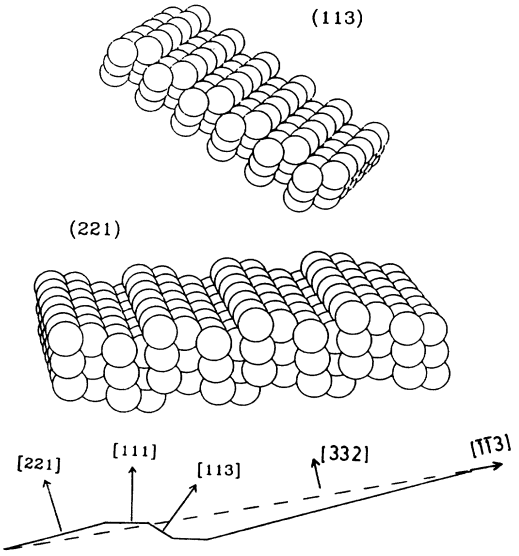


FIG. 7. Ball models of two of the facets identified on the Al(332) surface. The (113) and (221) surfaces may be compared directly with the upper part of Fig. 1, showing the ideal (332) surface. The surface profile at the bottom shows how the (332) macroscopic surface can be restructured to consist of (221), (111), and (113) facets without the presence of any (332) facets.

tively, can be anticipated on geometrical ground since the step heights on all these facets is the same ($h=2.36$ Å). Without a knowledge of the fractional coverage due to other facets, e.g., (332) facets, however, it is not possible to determine the absolute values of the $f$'s. The overall macroscopic surface must be maintained when averaged over large areas during the facetting process and the following simple relationship representing conservation of the total number of steps holds:

$$f_{(111)}\rho_{s(111)}+f_{(221)}\rho_{s(221)}=(f_{(111)}+f_{(221)})\rho_{s(332)} . \quad (2)$$

Since $\rho_{s(111)}$ is zero, then the relative concentrations of (111) to (221) facets are easily estimated from the known step densities $\rho_{s(221)}=0.833a^{-1}$ and $\rho_{s(332)}=0.520a^{-1}$ [$a=2.38$ Å, the row spacing in (111) terraces of Al] to be $5\frac{1}{3}$:$3\frac{1}{3}$. Figure 7 illustrates how the redistribution of steps with (111), (221), and (332) facets can maintain the macroscopic surface. However, this facetting process requires a considerable degree of mass transport. The extent of mass transport required is clearly facet-size dependent. That a considerable amount of mass transport takes place can be judged from the width of the diffraction peaks from the (111) facets. The very sharp peaks with $\Delta K_x \cong 0.05$ Å$^{-1}$ ($\Delta\theta=0.35°$, $k_i=6.67$ Å$^{-1}$), which are limited only by the experimental resolution, indicate (111) facets of dimension larger than $\sim 120$ Å. Similar estimates for the dimensions of the (221) or (332) faces are obscured by the overlapping of several peaks.

Since these measurements were restricted to one scattering plane, other facets having specular directions out of the scattering plane may well be present. Such facets [e.g., (131)] cannot show diffraction in the scattering plane of our experiment, except at the 3D Bragg conditions. To study the out-of-plane facets, measurements for a wide range of different azimuthal directions would be required. Such measurements are easily possible with the present apparatus, but have not yet been performed.

## IV. KINEMATIC APPROXIMATIONS

Figure 6 shows a qualitatively different intensity distribution than the LEED patterns, as illustrated in Figs. 2 and 3. This difference can be attributed to the different form factors in HAS compared to LEED. These differences in the form factors and the sensitivity of HAS only to the outermost layer of the surface also affect the way in which the intensities along reciprocal-lattice rods are modulated in the two different experiments.

We recall that electrons are scattered by the inner cores of the individual atoms. Thus, atoms at step edges scatter much the same as terrace atoms. Steps can thus only be detected by the phase differences of atoms on different terraces via the structure factor or by virtue of slightly different form factors. As opposed to electrons, He atoms are scattered from the relatively low electron densities at distances of the order of 6–7 a.u. from the atomic centers of the outermost plane. At these large distances the sum of the equipotentials on the densely packed surfaces [e.g., (111) and (100)] results in smooth potential surfaces with only very slight corrugations. This smoothing is enhanced by Smoluchowski electron smearing.[28] The diffraction intensities from these smooth surfaces are only $10^{-2}$–$10^{-3}$ of the specular intensity. Adatoms or steps produce much larger local corrugations with much larger scattering amplitudes. Steps have been shown to have a strong asymmetry in the form factors, which is related to the classical rainbow scattering from the sloped portions of the steps. Thus, for atoms approaching downward steps, scattering with positive momentum transfer $\Delta K_x$ predominates, while for scattering from upward steps scattering with negative momentum transfer is predominant.

For the one-dimensional case the He-atom-scattering amplitude consists of three contributions,[29]

$$A(\Delta\mathbf{k})=\frac{1}{L}\left[\sum_{l}^{T} F_{\mathrm{ter},l}(\Delta\mathbf{k})e^{i\Delta\mathbf{k}\cdot\mathbf{r}_l} + \sum_{m}^{U} F_{\mathrm{up}}(\Delta\mathbf{k})e^{i\Delta\mathbf{k}\cdot\mathbf{r}_m} + \sum_{n}^{D} F_{\mathrm{down}}(\Delta\mathbf{k})e^{i\Delta\mathbf{k}\cdot\mathbf{r}_n}\right], \quad (3)$$

where the total momentum transfer $\Delta\mathbf{k}$ is made up of the $x$ and $z$ momentum-transfer components, $\Delta\mathbf{k}=\Delta K_x\hat{\mathbf{x}}+\Delta k^z\hat{\mathbf{z}}$. $F_{\mathrm{ter},l}$ is the terrace form factor of the $l$th terrace from a total of $T$ terraces. $L$ represents the total length of a unit cell used to model a stepped surface of any given step-edge distribution. $F_{\mathrm{up}}$ and $F_{\mathrm{down}}$ are the form factors for scattering from step edges of up and down orientations, respectively. For a unit cell that conserves a low-index macroscopic plane, we have that the total number of steps down, $D$, equals the number of steps up, $U$, and is $T/2$. For an ideal stepped surface, either $D$ or $U$ may be zero; for a facetted surface the ratio of $D/U$ will reflect the macroscopic tilt of the surface. $\mathbf{r}_l$, $\mathbf{r}_m$, and $\mathbf{r}_n$ represent the coordinate vectors of the $l$th terrace, $m$th step up, or the $n$th step down, respectively.

Expression (3) can be greatly simplified. For uphill scattering with $\Delta K_x<0$ as used in the present experiments,

$$A(\Delta\mathbf{k})\cong\frac{1}{L}\sum_{m}^{U} F_{\mathrm{up}}(\Delta\mathbf{k})e^{i\Delta\mathbf{k}\cdot r_m} , \quad (4)$$

and all the other terms can be neglected. Thus HAS is, in this range of parallel momentum transfer, to a good approximation, only sensitive to step edges with one orientation and virtually insensitive to the terraces and step edges with the opposite orientation. As shown elsewhere, the scattering intensity from a single step shows broad undulations out to $|\Delta K_{\parallel}| \lesssim k_i$ with spacing depending on the step width[30] with intensities between $5\times10^{-4}$ and $5\times10^{-5}$ of the specular.

The differences in form factors discussed above have, however, important consequences on the way in which the structure factors are weighted. As mentioned previously, LEED scattering intensities are centered on the reciprocal-lattice rods of terraces. Since the form factor of every scattering core is identical, the form factor of an

individual 1D model terrace of length $Na$ takes the form[31]

$$F_N \sim \frac{\sin^2(\Delta K_x Na/2)}{\sin^2(\Delta K_x a/2)} . \quad (5)$$

This demonstrates that in LEED the width of the envelope of a diffraction feature in $K$ space, $\sigma_K$, is weakly dependent on the statistical distribution of terraces, but is necessarily closely related to the average distance between step edges, $\bar{s}$:

$$\sigma_K \sim 2\pi/\bar{s}, \quad \sigma_K \sim 2\pi/\bar{N}a , \quad (6)$$

as

$$\bar{s} \cong \bar{N}a . \quad (7)$$

Secondly, every terrace of a surface, or every facet vicinal to that terrace normal, produces LEED intensities close to most, if not all, reciprocal-lattice rods.

Unlike the LEED form factors, the HAS form factors for $\Delta K \neq 0$ are due almost entirely to the steps. Thus we expect the HAS intensity to be along the full length of the lattice rods of the macroscopic surface. This is clearly evident in Fig. 6, where the peak intensities are distributed along the entire length of the macroscopic step lattice rods. Thus the macroscopic step lattice rods show up much stronger in HAS than in LEED, explaining the striking sensitivity of HAS to facetting. Thus, with HAS, it is possible to identify all the types of occurring vicinal facets.

Recent LEED experiments from decorated vicinal surfaces[32] have been reported, showing the types of intensity patterns observable with He-atom scattering. Only under such conditions can LEED experiments begin to have the extreme sensitivity to disorder on vicinal surfaces and facets that is characteristic of HAS.

In the case of HAS the effect of the disorder of facets is now manifested along the corresponding facet lattice rods at positions between the 3D Bragg points at the anti-Bragg conditions.[33] Unfortunately, the phrase "anti-Bragg condition," denoted here $AB$, has come to mean two possible types of condition. The phraseology used in LEED studies is often inconsistent with that used for He-atom-scattering studies of vicinal surfaces. In HAS the $AB$ condition is fulfilled at a point halfway along the reciprocal-lattice rod of the macroscopic vicinal surface. In the (111) coordinate frame this corresponds to the condition $\Delta K_x = (2n+1)\pi/a$, where $n$ is an integer. This is a logical result of the ability of He-atom diffraction to see step-periodicity diffraction peaks along the full length of the reciprocal-lattice rods. Because of the different form factor, LEED intensities are restricted to regions around the $\Delta K_x = 2n\pi/a$ reciprocal-lattice rods. Thus, in LEED studies, $AB$ refers to the interterrace out-of-phase scattering condition. For the direction close to (terrace) specular, this implies the condition $\Delta k^z = (2n+1)\pi/h$ [see Fig. 2(a)]. In this paper we choose to use consistently the HAS definition of the $AB$ condition.

As in LEED, distributions in terrace lengths will lead to peak broadenings. In HAS the sensitivity to the terrace-length distribution is greatly enhanced. If one terrace in a facet is longer (shorter), then all the following step edges will also be shifted in the same direction. This phenomenon is expected from the repulsion and correlation of step edges.[34] The height of this shifted atomic layer will depend on the facet geometry. For a (111) terrace it is equal to a level spacing of $h = 2.34$ Å, but for a (221) facet it is 0.67 Å and for a (332) facet it is 0.43 Å.[35] Although much smaller than the (111) interlayer distance $h$, these corrugations will lead to considerable additional broadening of the macroscopic lattice rods. Thus the roughness of each facet provides a strong broadening which is greatest at the anti-Bragg condition and vanishingly small at the 3D Bragg conditions.

The above discussion has assumed the neglect of multiple-scattering processes.[36] These play an important role in LEED and make the dynamical electron-scattering problem exceedingly complicated.[37] For small corrugations it is well established that for He atoms multiple scattering can be neglected. For the present case of scattering from the large corrugation produced by uphill

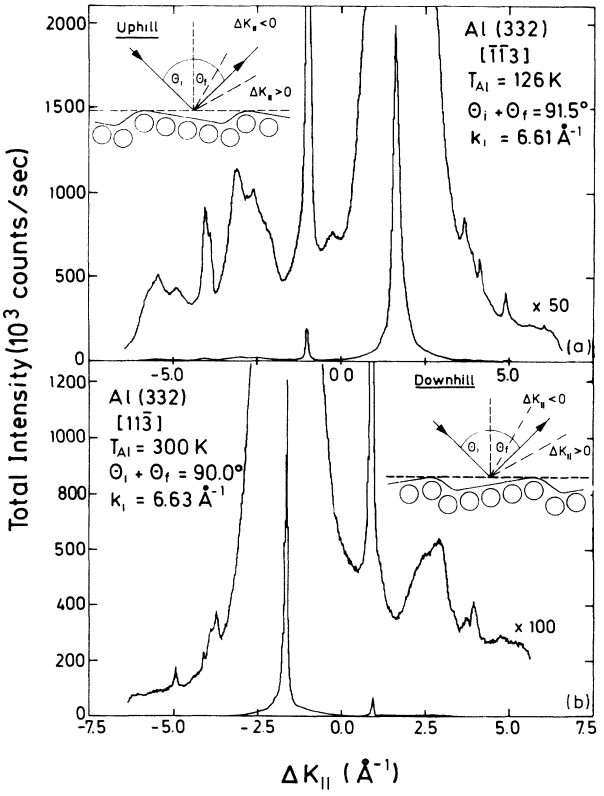


FIG. 8. Comparison of angular distribution measured under similar experimental conditions, but for two 180° azimuthally rotated scattering geometries. The two geometries are shown as insets. The present investigation deals mostly with the uphill scattering geometry. The total intensities are plotted as a function of parallel momentum transfer in the macroscopic surface coordinate frame. Note the different magnification factors (50× and 100×).

steps, this is not necessarily the case. To study the possible role of multiple scattering, we have carried out angular scan measurements for two different scattering geometries. Figure 8(a) shows the results of uphill scattering (shown in inset) perpendicular to the step edges, along the $\langle \bar{1}\,\bar{1}\,3 \rangle$ azimuth. The scan is made by rotating the crystal through 90°, between angles of grazing exit to angles of grazing incidence. A fixed detector and source dictate a constant total scattering angle, $\theta_i + \theta_f = 91.50$. The scan of Fig. 8(b) was taken under almost identical conditions, but in a quite separate apparatus. Here, $\theta_i + \theta_f = 90.0°$, but contrary to Fig. 8(a) the scattering was in the reverse direction (along the $\langle 11\bar{3} \rangle$ azimuth), or downhill, as illustrated in the inset. Absolute intensities and noise levels of the different systems vary, but the qualitative features of these scans are nearly identical. Differences are explained solely in terms of slightly different $k_i$ values or angular resolution for the two systems, and in different surface temperatures. This comparison shows that no complex mechanisms (e.g., multiple scattering) need be envoked to explain the scattered intensities. This indicates the general validity of neglecting multiple scattering for HAS studies of facetted surfaces even at extreme uphill geometries and/or for large scattering angles.

## V. THERMAL EFFECTS

In discussing the qualitative changes in the diffraction scans with increasing surface temperature, two effects must be accounted for. (1) The increase of thermal vibrations at higher surface temperatures $T_{Al}$ reduces the elastic scattering from the surface, $I = I_0 \exp[-2W(T_{Al})]$, where the Debye-Waller factor, $W(T_{Al})$, is expected to be of the same order of magnitude for each diffraction peak.[38] For the (111) specular peak for temperatures between 300 and 500 K, $W$ was found experimentally to be proportional to $T_{Al}$ with $\Delta W/\Delta T \cong 1.3 \times 10^{-3}$ K$^{-1}$ for the (111) specular peak. (2) Associated with the loss in elastic signal, there is a corresponding increase in the phonon inelastic signal which appears at angles on both sides of the diffraction peaks.[39] This can be distinguished from the true elastic intensity using the time-of-flight (TOF) capabilities of the apparatus. A full report of dynamical properties and of phonon modes identified from studies of the inelastic intensities is planned to be given elsewhere.[40] For our purpose here, the TOF analysis was used simply to ensure that the elasticity scattered component could be separated off from the inelastic HAS intensity.

The importance of this TOF analysis at elevated temperatures is illustrated in Fig. 9. There, an angular distribution measured without TOF analysis at the comparatively high crystal temperature of 606.4 K is compared with an angular distribution measured at room temperature. At the higher temperature the fraction of coherent elastically scattered intensity is significantly reduced by about a factor 2.5 compared to $T_s = 308$ K. Figure 10 shows a series of TOF spectra for surface temperatures between 180 and 600 K. At the higher temperature it is seen that the amount of inelastic scattering has increased

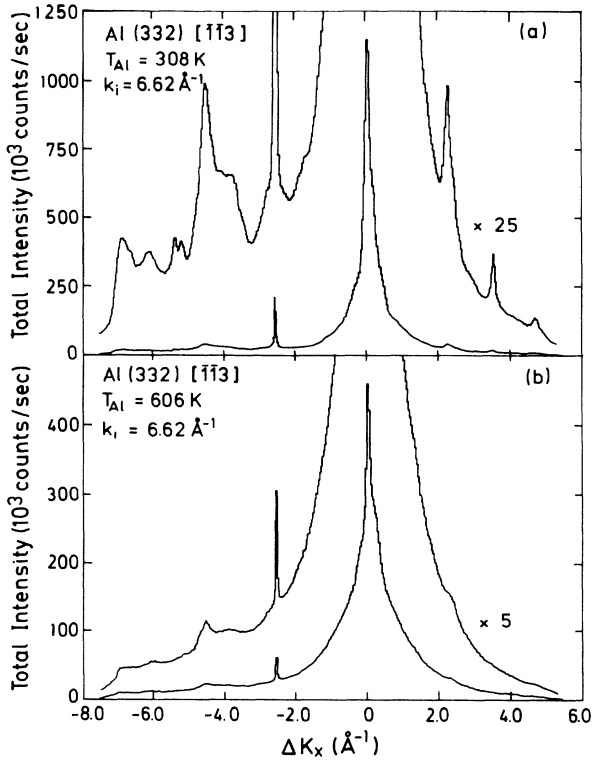


FIG. 9. Comparison of angular distributions of total scattered intensity for the Al(332) surface at (a) 308 K and (b) 606 K. Note that at the higher temperature most of the structure seen at room temperature has disappeared.

significantly, while the elastic peak has been diminished as a result of the Debye-Waller factor. Finally, in Fig. 11 a comparison of the elastic intensities taken from the TOF spectra after subtracting off the interpolated multiphonon background is presented for the same temperatures and wave vectors as in Fig. 9. The elastic angular distribution shown in Fig. 11(b), although now a small proportion of the total HAS intensity, contains much more structure and is, in fact, very similar to the elastic distribution at 300 K. Thus the broadening and smearing out of the feature in Fig. 9(b) is not due to any structural changes of the surface, but is simply due to an increase in the inelastic scattering in the angular distributions measured without TOF analysis. This is clear evidence that TOF energy resolution is essential in order to obtain structural information with quantitative accuracy. A similar investigation is reported in Ref. 41 for the study of the thermal roughening. Another attempt to separate inelastic-scattering intensity has been done by Engel *et al.*,[42] but with an energy resolution which is an order of magnitude less than these measurements.

This technique has been used to measure the FWHM of diffraction peaks in the region $\Delta K = -2.5$ Å$^{-1}$. The results are plotted as a function of the crystal temperature in Fig. 12. The one peak at $\Delta k^z = 8.86$ Å$^{-1}$ (triangles) corresponds to a 3D Bragg condition of the specular peak of the (221) facet and $\bar{1}0$ peak of the (111) face. As expected from the properties of the 3D Bragg points, this

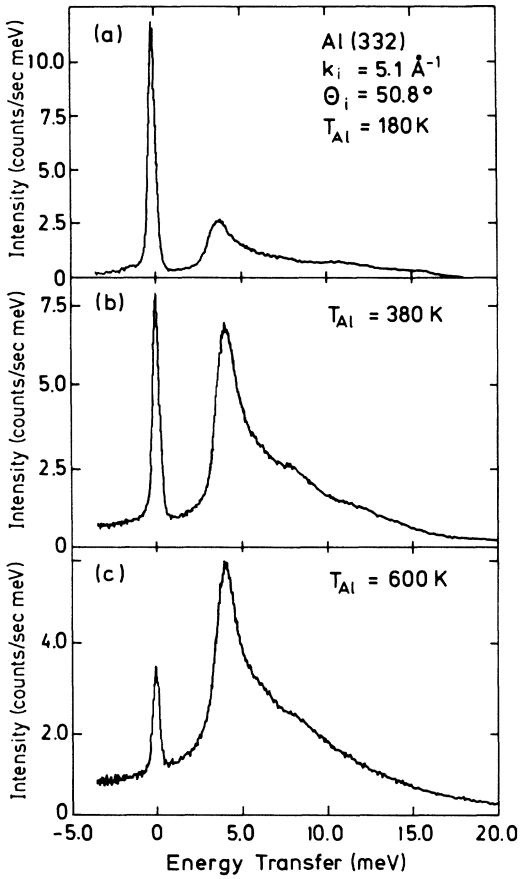


FIG. 10. Series of time-of-flight spectra taken at the same kinematical conditions, but for different surface temperatures. At 180 K the elastic peak at $\Delta E=0$ meV predominates. With increasing temperature the inelastic peak increases in intensity. At the highest temperature the area under the inelastic portion of the time-of-flight spectrum is much larger than that in the elastic peak.

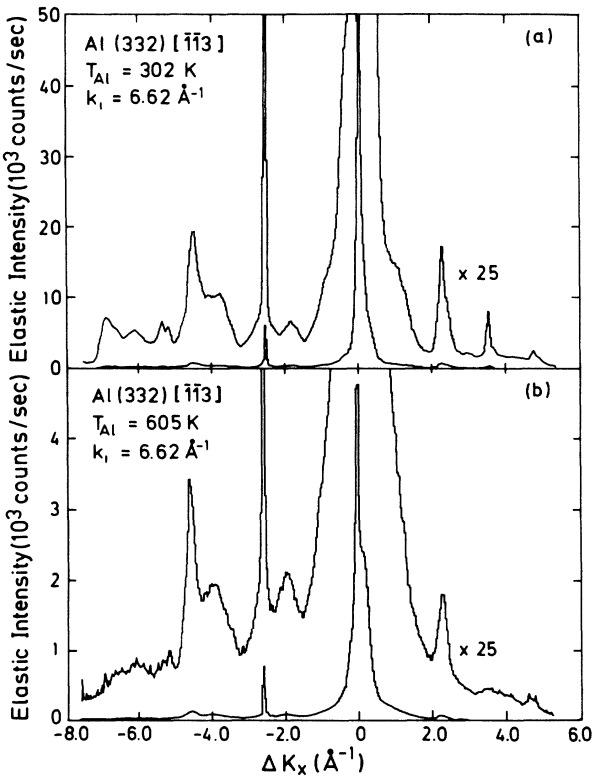


FIG. 11. Comparison of angular distributions of the elastic peaks taken from TOF spectra similar to those shown in Fig. 10. After the removal of the inelastic intensities, it is surprising to find that the elastic angular distribution at the two temperatures now appears to be very similar and that the structure lost at the higher temperature in the total intensity angular distribution of Fig. 9(b) is recovered. Note, however, that the absolute elastic intensity at 605 K, (b), is down by an order of magnitude compared to 302 K, (a).

peak is insensitive to the surface temperature. The constant width of this peak in reciprocal-lattice space, $\Delta K_x=0.06$ Å, compares well with the angular resolution of the apparatus, $\Delta\theta=0.35°$. This result illustrates once more that the sharpest peaks at the 3D Bragg points are insensitive to virtually all types of surface disorder. In contrast, curves composed of circles and squares are for two peaks that are roughly midway between 3D Bragg conditions. The peak which is denoted by squares is identified as the first-order peak; the one which is denoted by circles is the second-order diffraction peak from the (221) facets. Both peaks have perpendicular momentum transfers [relative to the (111) coordinate frame] of about 13.0 Å$^{-1}$, which for a (111) surface would be described as an anti-Bragg condition (LEED definition). These peaks show a measurable broadening over this temperature range and are hence sensitive to an increasing surface roughness. The two curves in Fig. 12 (○,□) demonstrate that the roughness of (221) facets increases continuously in the range 300–600 K. Thus the surface changes over this temperature range, indicating a mobility of step edges. In this range of temperatures the disorder is apparently not frozen in.[43] Measurements were not performed systematically at lower temperatures, but the available data suggest that the half-widths will always be greater than the angular resolution. This is consistent with the idea that the surface will have a certain amount of disorder, even at lower temperatures.

## VI. SURFACE-FACET STABILITY

At low incident energies and high crystal temperatures another qualitative change in the angular distributions is seen. Figure 13 illustrates the appearance of a previously unobserved peak maximum in a direction close to the (111) specular one as the crystal temperature is raised. Again, careful study of this peak with varying incident wave vector recorded using the TOF energy discrimination to separate off the elastic peak reveals that the elastic-peak position runs at an angle of $\sim 10°\pm 0.5°$ to the (111) reciprocal-lattice rod (see Fig. 14). The new feature, which is sharpest at 650 K, has been identified as the third-order diffraction peak from (332) facets of the surface. It was the first evidence encountered in these experiments for (332) facets.

This new (332) feature is observed most clearly at low

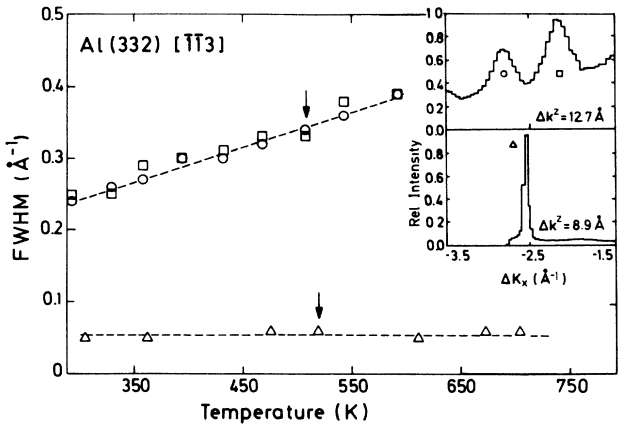


FIG. 12. Full widths at half maximum (FWHM) of the widths of two characteristic elastic diffraction peaks are plotted as a function of increasing surface temperature. All elastic intensities were determined from TOF spectra and fits were made to the data assuming simple Gaussian peak shapes. Triangles: 3D Bragg condition, $\Delta k^z = 8.86$ Å$^{-1}$, $\Delta K_x = -2.55$ Å$^{-1}$. Circles: $\Delta k^z = 12.62$ Å$^{-1}$, $\Delta K_x = -2.88$ Å$^{-1}$. Squares: $\Delta k^z = 12.78$ Å$^{-1}$, and $\Delta K_x = -2.22$ Å$^{-1}$. The inset shows two typical angular scans at $\Delta k^z \approx 12.7$ Å$^{-1}$ (top) and $\Delta k^z \cong 8.9$ Å$^{-1}$ (bottom), both taken at surface temperatures of about 510 K, as indicated by the black arrows. At the 3D Bragg condition (△) the peak width is not affected by temperature-induced disorder, whereas at kinematic conditions near the anti-Bragg condition (○,□) a temperature-dependent broadening of the peaks is observed.

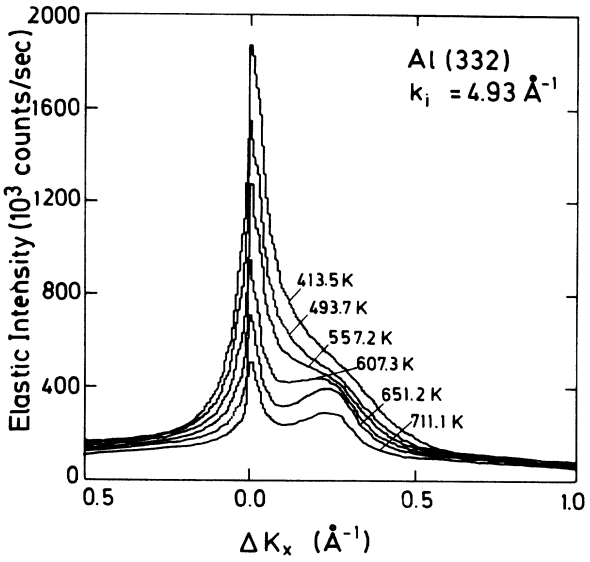


FIG. 13. Angular distributions of elastic scattered intensities measured close to the terrace specular direction are plotted for a series of increasing surface temperatures. With increasing temperatures, a well-defined peak develops at $\Delta K_x = 0.25$ Å. As shown in Fig. 14, this peak has been identified as the (332)-surface third-order diffraction peak.

incident-beam energies. The extra peak is estimated to have its greatest in-plane intensity at $k_i \approx 5.1$ Å$^{-1}$ or $\Delta k^z \approx 7.2$ Å$^{-1} \pm 2\%$. At this incident energy the third-order (332) diffraction peak is roughly 1.25° ($\Delta K_x = 0.17$ Å$^{-1}$) from the true (111) specular direction. Maximum intensities from vicinal superlattice diffraction peaks are normally expected to coincide with the terrace (111) specular direction (or 3D Bragg condition). At low incident energies, however, the presence of an energetic well in the He-atom–surface interaction potential will influence the trajectories considerably. A similar effect was found, and a similar interpretation given for large-angle HAS results from a Pt(997) surface.[44] With increasing well depth, the classical terrace rainbow direction was found to move (for uphill scattering) to more negative $\Delta K_x$. The same effect is expected to occur in the present experiments. A shift in scattering angles will influence the position in both directions in the $\Delta k^z, \Delta K_x$ plane. Using a model of the vicinal (332) surface with a potential well similar to the model of Harris *et al.*,[45] it was possible to explain the shift away from the 3D Bragg condition by a potential-well-depth value of only about 1.7 meV. In this simple estimate the disorder-induced broadening due to step edges was, however, ignored. Moreover, only the in-plane intensities were observed, and for an accurate comparison the out-of-plane scattering should be taken into account. Simple geometrical considerations suggest that the use of in-plane intensities alone underestimate the angle between the maximum in-

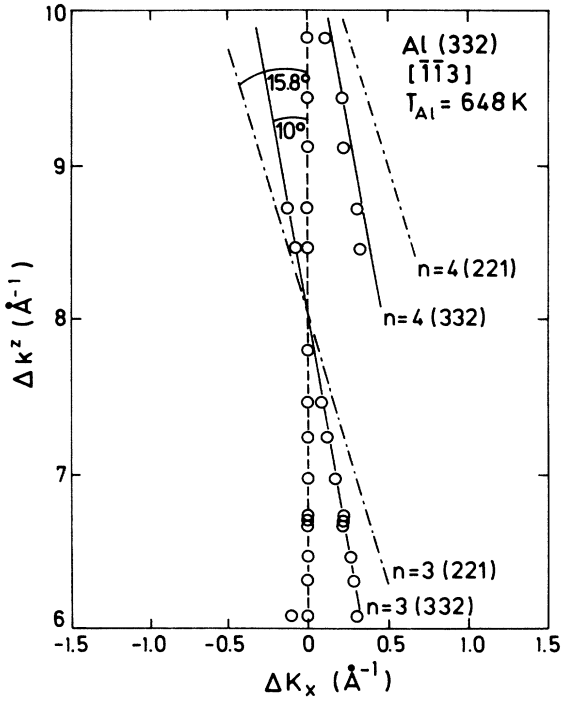


FIG. 14. Total intensity maxima positions as observed at an elevated surface temperature of 648 K. For this plot incident energies vary between 9.6 and 23.3 meV. The vertical dashed line indicates the (111) terrace (facet) specular reciprocal-lattice rod. The two solid lines, indicating the third- and fourth-order lattice rods of the (332) surface, coincide well with the feature which grows at this surface temperature. For comparison, the third- and fourth-order reciprocal-lattice rods of the (221) facets are also shown as dashed-dotted lines.

tensity peak and (111) specular direction (here 1.25°). The value of 1.7 meV must then be an underestimate of the true well depth.

The isolated observation of a (332) feature opens up the possibility of studying its behavior with changes of temperature. Prior to all of the following measurements, the crystal was first rapidly ( ~300 sec) flashed to 720 K and then the heating was switched off, so that the crystal cooled to room temperature or somewhat below ( ~600 sec) to ensure a reproducible initial structure. Figure 15 displays the total intensity measured at the same third-order (332) superlattice peak maximum, both before and after Debye-Waller correction, during a slow temperature cycle (350→650→350 K) over a total time of 60 min. The Debye-Waller factor was obtained from the intensity change observed during heating at temperatures below 500 K. In this slow annealing the intensity from the (332) facet starts to rise at about 550 K and reaches a maximum at 630 K. An analysis of the time response revealed that the greatest rate of change occurred at 570 K. At temperatures greater than 630 K the (332) intensity drops off sharply, indicating a temperature-induced facetting out of the (332) structure. During the subsequent cooling the intensity recovers and the maximum is nearly maintained in the slow cooling down to the lowest temperatures. Thus, in this case some of the original macroscopic (332) surface is recovered.

For comparison, Fig. 16 shows analogous curves for a more rapid temperature cycling taken over a shorter, 10-min, total cycle time which reveal a different behavior. In the initial heating phase a maximum of the density of (332) facets is again produced at about the same temperature of 630 K, but the intensity increase is about 50%

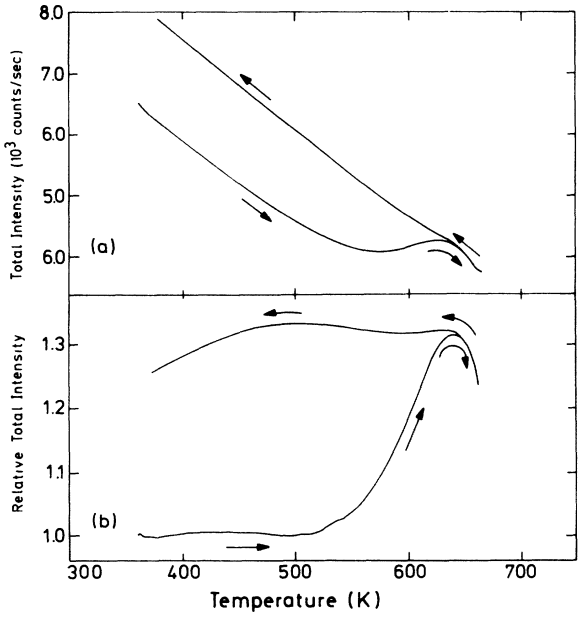


FIG. 15. Temperature dependence of the third-order (332) diffraction peak total intensity. Curve (a) shows the intensity during a temperature cycle from 300→650→300 K over 60 min. Curve (b) shows the same intensity after a Debye-Waller correction.

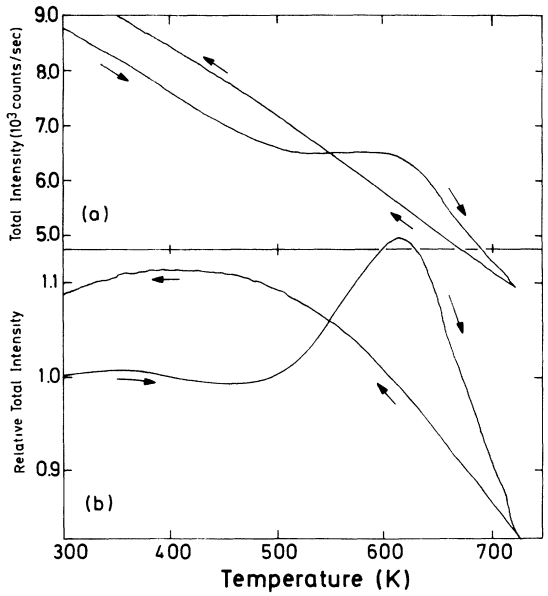


FIG. 16. Same as Fig. 15, but for a fast 720-K flash and rapid cooling with liquid nitrogen. The initial temperature of 300 K was again reached after 10 min. Curves (a) and (b) are again the total intensities before and after the Debye-Waller correction.

smaller. This would suggest that the time was much too short to reach equilibrium. Upon cooling, the maximum intensity is not recovered at 630 K, but only at about 500 K, corresponding to the initial increase in the heating phase. In this case insufficient time is available for the restructuring to fully occur in the heating cycle, and only with considerable temperature lag in the cooling cycle. It is clear that the formation of (332) facets is rate-limited, and equilibrium facet distributions are not achieved during rapid temperature changes. The hysteresis of the intensity, seen during the cycling of surface temperature, must be associated with a rate-dependent irreversibility in the relative proportions of facets, $\{\rho\}$.

With the same starting surface condition, described above, the proportional increase of the (332) feature has been measured at 350 K as a function of the maximum anneal temperature (Fig. 17). The heating conditions were similar to those of the fast cycling in Fig. 16 and nearly identical for each point. Once the desired temperature was reached, the heating was switched off, allowing the sample to cool again to room temperature. This cooling typically took 10 min and corresponds closest to the cooling in the fast cycling described above. At annealing temperatures less than ~610 K the proportion of (332) facets was observed to increase with increasing annealing temperature. At higher annealing temperatures it decreased. For these experiments the heating was relatively fast and the surface response is too slow to reach an equilibrium state. The maximum increase obtained was only about 14%. During the slow anneal cycles (e.g., Fig. 15) the proportional increase of the (332) superlattice peaks was as large as 35%. The limiting factor is probably the diffusion rate at these temperatures for the large degree of mass transport required in facet redistribution. From

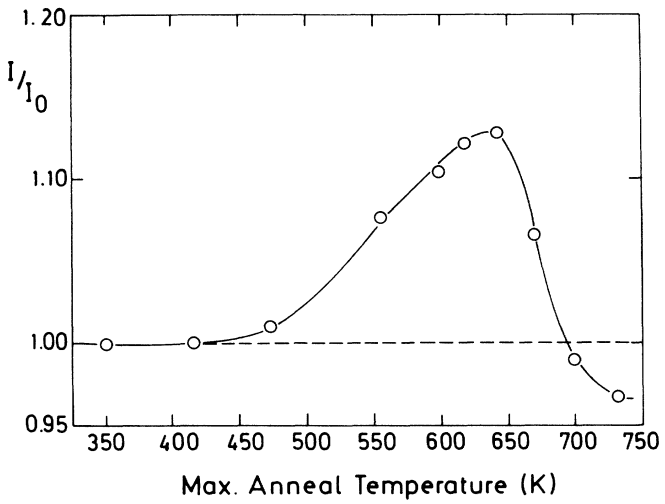


FIG. 17. Ratio of intensities of the third-order peak from the (332) surface after and before annealing as a function of the maximum annealing temperature. All intensities were measured at 350 K. The curve illustrates the nature of a hysteresis after a heating cycle (at constant heating power) to the maximum indicated temperatures.

the very slowest temperature cycles (total time 300 min) a maximum in the intensity increase with time was observed at 570 K. The observed intensity changes with time were used to determine rates, and from an Arrhenius plot in the temperature range 500–565 K the activation energy for reordering diffusion was estimated to be $0.17\pm0.03$ eV. (Unfortunately, we have not found any values in the literature for comparison.) This value is expected to have additional large systematic errors because of uncertainties in the Debye-Waller correction. We note that the observed facet reordering will involve many different elementary processes and not simply the motion of adatoms on (111) terraces.

The thermal behavior of the Al(332) surface can thus be divided into three regimes. At high temperatures ( $>640$ K) the thermodynamical most favorable phase involves apparently (221) and (111) facets. These are the facets observed at room temperature (Fig. 6), which have been apparently frozen in by the rapid cooling used in preparing the crystal. In the intermediate range ($640 < T_{\mathrm{Al}} < 500$ K) a partial reordering to the macroscopic (332) surface occurs. At lower temperatures the (221) and (111) facets are frozen in and the restructuring of the (332) facets is inhibited. It is interesting to compare this observation with the conclusions drawn from Fig. 12, i.e., that the (221) facets become continuously rougher with increasing temperature, indicating a mobility over the full 300–600 K range. The processes of facetting and roughening are, in fact, quite separate phenomena. The extent of mass transport required for step-edge roughening is orders of magnitude smaller than that for facet building. Presumably, the energetics for both processes will also be quite different.[46] In both processes the thermal activation energy is necessary, but in the case of facetting the facets are also stable after cooling, while the roughening is reversible.

Testoni and Stair[47] have reported thermal instabilities on the smooth Al(111) surface, which show the tendency to build (221) facets. Their work advocates a very long (slow) annealing process to form a well-prepared (111) surface. From their studies it is not clear whether at high temperatures ( $>650$ K) facets on the Al(111) surface anneal out or whether the surface condition is improved, presumably during the slow cooling. These two possibilities may be relevant to our interpretation of what happens on the (332) surface. The high-temperature facetting process may be driven by the greater stability of either of the (111) or (221) faces. It is the former that seems more realistic, on the grounds that the (221) facets are still very rough. This rough facet may contain regions which are still locally (332). At surface temperatures less than 640 K the (332) face is more stable than a linear combination of (111) and (221) facets.

The above temperature-cycling experiments suggest an optimal temperature cycling for obtaining (332) facets. This treatment should involve a flash to 620 K and then a slow cooling to room temperature. The diffraction pattern obtained at room temperature after this treatment is shown in Fig. 18(b). A small sharp shoulder is now observed at about $\Delta K_x = 0.2$ Å$^{-1}$ similar to what was found in the elastic peak after the high-temperature cycling

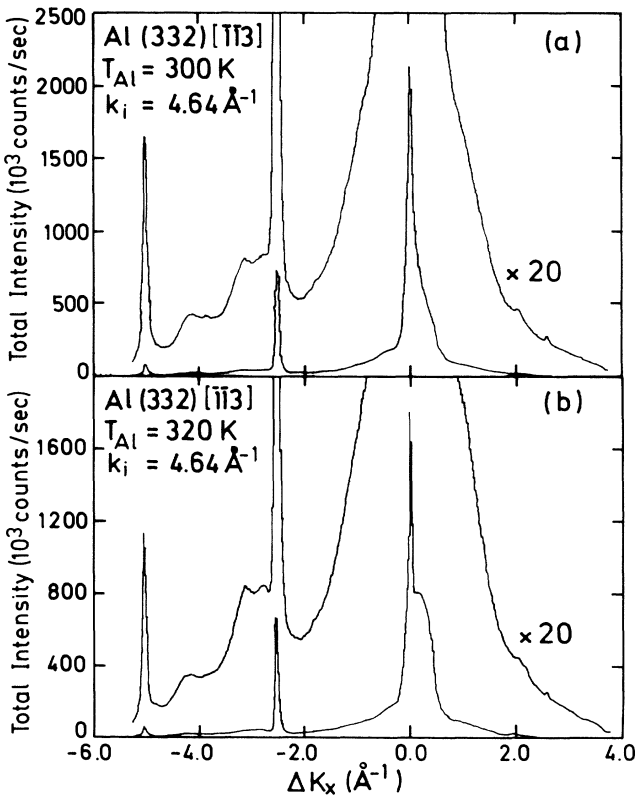


FIG. 18. Comparison of angular distribution of total intensities observed after rapid and slow cooling. (a) Fast temperature flash to 720 K and immediate cooling. (b) Flash to 620 K and slowly cooled, over 60 min, to room temperature. The long annealing treatment induces new structure, near the terrace specular direction, which is identified as a (332) diffraction feature.

shown in Fig. 13. As shown in Fig. 18(a), this peak is not found when the crystal is flashed to 720 K and cooled immediately. Since this is the procedure used in the measurements described in the first part of this article, this observation explains the lack of any evidence for the (332) faces in our other experiments.

At no stage was a surface prepared which exhibited (111) specular spot splitting, however. Thus it would appear that a considerable proportion of the crystal surface remains as (111) facets.

Adsorbates are known to induce facetting on many surfaces.[12,13,17–19] After either slow- or fast-cycling procedures the surface contaminant levels, as measured by x-ray-photoemission spectroscopy at surface temperatures of under 350 K, remained less than 0.3%. The possibility of reversible surface segregation and incorporation processes of bulk contaminants must nevertheless be considered. We deem this unlikely, since such a segregation, occurring only in the temperature range 550–640 K, must be of insufficient quantities to drive the (332) stabilization, and incorporation must occur again at $T \ll 550$ K. Instead, we believe the observed thermal behavior to be a property of the clean Al(332) surface.

## VII. SUMMARY

Data have been presented that illustrate the strength of HAS as a diffraction tool in identifying complex morphologies of crystalline surfaces. For metallic surfaces with close-packed terraces, the scattering from HAS is divided into two distinct regions. The scattering close to the terrace specular direction can yield much the same information as LEED studies. In contrast, the large-angle scattering is dominated by step-edge diffraction, which has no kinematic analog in LEED. The large-angle-scattering intensities are not restricted to regions close to $\Delta K_x = G_x$ conditions, but can be found at almost all kinematic conditions. This implies a considerably enhanced sensitivity to facet orientations, and also to disordering on each of the facet types.

With the aid of TOF energy resolution, the disordering and ordering processes on an Al(332) surface have been studied. Increasing disorder in individual facets as well as the complete redistribution of facets has been observed with increasing temperature. The true Al(332) face has been shown to exhibit three distinct temperature regimes, indicating a complex dependence of surface energies with temperature.

## ACKNOWLEDGMENTS

One of us (B.J.H.) wishes to thank the Alexander von Humbolt Foundation for support.

*Present address: Bell Laboratories, 600 Mountain Avenue, Murray Hill, NJ 07974.

†Present address: Fritz-Haber-Institut, Faradayweg 4-6, 1000 Berlin 33, Federal Republic of Germany.

[1]G. A. Somorjai, *Chemistry in Two Dimensions: Surfaces* (Cornell University Press, Ithaca, NY, 1981), and references therein.

[2]M. K. Debe and D. A. King, Surf. Sci. **81**, 193 (1979).

[3]R. A. Barker and P. J. Estrup, J. Chem. Phys. **74**, 1442 (1981).

[4]W. Telieps and E. Bauer, Ultramicrosc. **17**, 51 (1985).

[5]J. F. Wendelken and G. C. Wang, Phys. Rev. B **32**, 7542 (1985).

[6]H. Pfnür (unpublished).

[7]F. Fabre, B. Salanon, and J. Lapujoulade, Solid State Commun. **64**, 1125 (1987); F. Fabre, D. Gorse, B. Salanon, and J. Lapujoulade, J. Phys. (Paris) **48**, 1017 (1987); B. Salanon, F. Fabre, J. Lapujoulade, and W. Selke, Phys. Rev. B **38**, 7385 (1988).

[8]E. Conrad, R. Aten, D. Kaufman, L. Allen, T. Engel, M. den Nijs, and E. Riedel, J. Chem. Phys. **84**, 1015 (1986); J. Chem. Phys. **85**, 4756 (1986); E. Conrad, L. Allen, D. Blanchard, and T. Engel, Surf. Sci. **187**, 265 (1987); D. Kaufman, R. M. Aten, E. H. Conrad, L. R. Allen, and T. Engel, J. Chem. Phys. **86**, 3682 (1987).

[9]A. Bartolini, F. Ercolessi, and E. Tosatti, Phys. Rev. Lett. **63**, 872 (1989).

[10]G. Comsa, G. Mechtersheimer, and B. Poelsema, Surf. Sci. **97**, L297 (1980).

[11]G. Comsa, G. Mechtersheimer, and B. Poelsema, Surf. Sci. **119**, 159 (1982).

[12]B. Lang, R. W. Joyner, and G. A. Somorjai, Surf. Sci. **30**, 454 (1972).

[13]D. W. Blakely and G. A. Somorjai, Surf. Sci. **65**, 419 (1977).

[14]P. W. Davies and R. M. Lambert, Surf. Sci. **110**, 227 (1981).

[15]H. V. Thapliyal and J. M. Blakely, J. Vac. Sci. Technol. **15**, 600 (1978).

[16]R. C. Cinti, T. T. A. Nguyen, and Y. Capiomont, Surf. Sci. **134**, 755 (1983).

[17]J. C. Boulliard, J. L. Domange, and M. Sotto, Surf. Sci. **165**, 434 (1986).

[18]J. C. Boulliard and M. P. Sotto, Surf. Sci. **177**, 139 (1986).

[19]M. G. Barthes-Labrousse, Surf. Sci. **177**, 338 (1986).

[20]M. Salmeron, B. Marchon, S. Ferrer, and D. S. Kaufman, Phys. Rev. B **35**, 3036 (1987).

[21]M. Sotto and J. C. Boulliard, Surf. Sci. **214**, 97 (1989).

[22]A. Lock (unpublished).

[23]J. P. Toennies, in *Surface Phonons,* edited by W. Kress (Springer, Berlin, 1990), Chap. 5.

[24]B. J. Hinch, D. R. Frankl, and W. Allison, Surf. Sci. **180**, 371 (1987).

[25]M. Henzler, Appl. Surf. Sci. **11/12**, 450 (1982).

[26]T.-M. Lu and M. G. Lagally, Surf. Sci. **120**, 47 (1982).

[27]G. Brusdeylins, R. B. Doak, and J. P. Toennies, J. Chem. Phys. **75**, 1784 (1981).

[28]R. Smoluchowski, Phys. Rev. **60**, 661 (1941).

[29]B. J. Hinch and J. P. Toennies, Phys. Rev. B **42**, 1209 (1990).

[30]A. M. Lahee, J. R. Manson, J. P. Toennies, and Ch. Wöll, Phys. Rev. Lett. **57**, 471 (1986).

[31]M. Henzler, Surf. Sci. **19**, 159 (1970).

[32]M. Henzler, in *Proceedings of the NATO Advanced Research Workshop on Kinetics of Ordering and Growth at Surfaces* (Plenum, New York, 1990).

[33]Figure 6 illustrates that the diffracted intensity from the Al(332) surface is made up of a superposition of diffracted intensities from three different facets. The reciprocal-lattice rods are seen to cross one another at the 3D reciprocal-lattice points. In fact, at these conditions all possible facets of the surface diffract into the same directions. For example, at an

incident wave vector of $k_i = 6.67$ Å$^{-1}$ (23.25 meV) the first-order diffraction from (111) facets and the zeroth-order diffraction from (221) facets coincide and these two peaks are indistinguishable at the three-dimensional (3D) Bragg condition. Note that this discussion only considers the intensities but not the phases of the individual scattered beams. The same 3D Bragg condition is also satisfied by considering the constructive (in-phase) scattering from any rough surface. In that case a sharp diffraction peak at the 3D Bragg points comes from the *coherent* addition of scattering amplitudes from many randomly distributed terraces.

[34]V. L. Pokrovskii and A. L. Talanov, Zh. Eksp. Teor. Fiz. **78**, 269 (1980) [Sov. Phys.—JETP **51**, 134 (1980)].

[35]For illustration, see Fig. 4 of Conrad *et al.*, J. Chem. Phys. **84**, 1015 (1986).

[36]T. Engel and K. H. Rieder, in *Structural Studies of Surfaces,* Vol. 91 of *Springer Tracts in Modern Physics,* edited by K. Heinz and K. Müller (Springer, Berlin, 1982).

[37]J. B. Pendry, *Low Energy Electron Diffraction* (Academic, London, 1974).

[38]J. Lapujoulade, Y. Lejay, and G. Armand, Surf. Sci. **95**, 107 (1980).

[39]R. Manson and V. Celli, Surf. Sci. **24**, 495 (1971).

[40]B. J. Hinch, A. Lock, H. H. Madden, J. P. Toennies, and G. Witte (unpublished).

[41]P. Zeppenfeld, K. Kern, R. David, and G. Comsa, Phys. Rev. Lett. **62**, 63 (1989).

[42]E. H. Conrad, L. R. Allen, D. L. Blanchard, and T. Engel, Surf. Sci. **198**, 207 (1988).

[43]F. Fabre, D. Gorse, B. Salanon, and J. Lapujoulade, Surf. Sci. **175**, L693 (1986).

[44]G. Comsa, G. Metersheimer, and B. Poelsema, Surf. Sci. **119**, 172 (1982).

[45]J. Harris, A. Liebsch, G. Comsa, G. Mechtersheimer, B. Poelsema, and S. Tomoda, Surf. Sci. **118**, 279 (1982).

[46]To estimate the relative energies for roughening and facetting, we thus note that roughening requires the overcoming of the kink-creation energy $W_{\text{kink}}$ and the step-step repulsion energy $W_{\text{step}}$. In the case of the Cu(113) and Cu(115) faces, Fabre *et al.* [F. Fabre, D. Gorse, J. Lapujoulade, and B. Salanon, Europhys. Lett. **3**, 737 (1987)] found for (113), values of $W_{\text{kink}} = 69$ meV and $W_{\text{step}} = 48$ meV, and, for (115), $W_{\text{kink}} = 60$ meV and $W_{\text{step}} = 12$ meV, respectively. We next estimate the facetting energy as follows. A possible driving force for facetting is the lowering of the surface tension. The difference in surface tension is assumed equal to the facetting energy. McLean [M. McLean, Acta Metall. **19**, 387 (1971)] reported for the Cu(100) surface a surface tension of approximately $\gamma = 1.67$ J/m$^2$, and observed an anisotropy of about 15% in $\gamma$ between the (100) and (110) poles of the sterographic projection. As a rough estimate, we assume a similar change in going from the (111) to the (115) surface. For one surface unit cell this corresponds to a change in the energy of about 0.12 eV during facetting. For a facet with a length of 100 Å, the corresponding surface tension is thus changed by about 3 eV. Although the energy change and mass transport depend on the size of the facets formed and the material, it would appear safe to assume that the facetting energy is at least an order of magnitude greater than the roughening energy.

[47]A. L. Testoni and P. C. Stair, Surf. Sci. **171**, L491 (1986).